Low-Complexity Multistep Model Predictive Current Control for Linear Induction Machines

Wei Xu, *Senior Member, IEEE*, Dinghao Dong, Jianqiao Zou, and Yi Liu, *Senior Member, IEEE*

***Abstract*—In this article, the predictive horizon of model predictive current control (MPCC) is extended for achieving better operational performance. However, the computational burden of MPCC exponentially increases with its predictive steps, and thus, the predictive step is usually chosen as one. In order to explore the potential advantage of multistep MPCC (M-MPCC), one simplified search method is proposed so that the M-MPCC can be executed in practice with greatly reduced complexity. In the proposed search method, a large number of possible voltage vector sequences can be excluded in advance with the guide of the defined reference voltage vector sequence. Then, one simplified M-MPCC is applied to two 3 kW arc induction machines with a large radius, which can make a full demonstration on the drive performance of linear induction machine in practice. The comprehensive simulation and experiments have clearly indicated the relationship between the predictive step and the performance of the proposed M-MPCC. It has persuasively verified the feasibility of low complexity and decreasing time consumption based on the proposed search method in this work.**

***Index Terms*—Linear induction machine (LIM), model predictive current control (MPCC), multistep MPCC (M-MPCC).**

I. Introduction

THE common rotatory induction machine (RIM) drive systems need the transformation gearbox to achieve the linear motion, which may decrease its transfer efficiency. In order to directly produce the linear movement, the linear induction machine (LIM) is derived from RIM by changing its magnetic structure [1], [2]. And it can be utilized in practical horizontal conveyance applications, such as metro, elevator, conveyor, aircraft launch, and so on [3], [4]. Due to the cut-open magnetic circuit in primary, the longitudinal end effect (LEE) of LIM would decrease the air-gap flux by inducing the entry end eddy current. Fortunately, many articles have studied the equivalent circuits of LIM to compensate the LEE [5]–[9].

Manuscript received June 1, 2020; revised October 8, 2020; accepted November 26, 2020. Date of publication December 9, 2020; date of current version March 5, 2021. This work was supported in part by the National Natural Science Foundation of China under Grants 51877093 and 51707079, in part by the National Key Research and Development Program of China under Grant 2018YFE0100200, and in part by the Key Technical Innovation Program of Hubei Province under Grant 2019AAA026. Recommended for publication by Associate Editor T. Shi. *(Corresponding author: Dinghao Dong.)*

The authors are with the State Key Laboratory of Advanced Electromagnetic Engineering and Technology, School of Electrical and Electronic Engineering, Huazhong University of Science and Technology, Wuhan 430074, China (e-mail: weixu@hust.edu.cn; dinghaodongee@foxmail.com; jianqiaozou@hust.edu.cn; liuyi82@hust.edu.cn).

Color versions of one or more figures in this article are available at https://doi.org/10.1109/TPEL.2020.3042660.

Digital Object Identifier 10.1109/TPEL.2020.3042660

The traditional control strategies for LIM come from the popular methods for RIM, such as the field-oriented control (FOC) and direct thrust control (DTC) [10]–[12]. These control methods, however, are just suitable for the case that the mutual inductance is unchanged. And thus, under the control of FOC or DTC, the variable mutual inductance caused by LEE may degrade the control performance. Recently, the model predictive control (MPC) is applied to LIM so as to compensate its LEE [13], [14], and the variable law of mutual inductance can be achieved by the correction coefficients proposed by Xu *et al.* [4]. The MPC incorporated with the reasonable equivalent circuit can well predict the future working state of LIM, and thus is a potentially suitable control method for the LIM drive systems.

The finite control set MPC (FCS-MPC) can directly determinate the switching state of the inverter without the need for a modulator, which can obtain the low switching frequency even with a high sampling frequency. However, it enumerates and evaluates all possible candidate voltage vectors (CVVs) to find the optimal one, resulting in a heavy computational burden. And thus, many simplified search methods have been proposed to reduce the complexity of MPC with one predictive step [15]–[17]. The more predictive steps of FCS-MPC will bring better performance, e.g., the smaller current total harmonic distortions (THDs) at low switching frequency [18]. The continuous control set MPC can simply increase its predictive step without the influence on its calculating cost since it has an explicit solution instead of by exhaustive computation [1]. However, in the case of FCS-MPC, the number of CVV sequence (CVVS) will exponentially increase with its predictive steps, and thus, the multistep FCS-MPC may need the high calculation cost to find the optimal solution in real applications.

In high-power applications, such as linear metro drive systems, the switching frequency is usually limited within a few hundred hertz. In this case, the multistep FCS-MPC can be explored so as to further optimize the relation between the current THD and switching frequency. Due to the heavy computational burden and some other problems, the multistep FCS-MPC has not been widely used in practical systems so far. In order to reduce the online calculating time of multistep FCS-MPC, many simplified search methods have been proposed, which can effectively avoid enumerating and evaluating all possible CVVSs. Among them, two typical simplification methods named branch and bound (BAB) method [19] and sphere decoding algorithm (SDA) [18] have attracted lots of attention. The idea of these two methods is approximately the same, which is similar to the online dynamic elimination. For the BAB method, the simplification

efficiency is related to the sequence search order. In [19], the predictive horizon is simply extended by extrapolating the control states trajectory, and its calculating cost can be further reduced by the BAB method. Therefore, this approximate method can acquire a very long predictive horizon without evaluating each predictive step by the cost function. The SDA adopts the notion of BAB and only considers the CVVSs within the sphere of current radius [20], [21]. The computational burden of SDA depends on the given radius, and the smaller radius will remove the more CVVSs, while too small radius may lead to an empty solution. Therefore, many principles till now have been proposed to select a suitable radius, such as the educated-guess method and the box-constrained quadratic programming method [22]. The results have shown that the selective initialization approach enables the deterministic use of multistep FCS-MPC no matter what conditions the drive encounter. In [21], a multistep MPC method for cascaded H-bridge inverters is proposed. To reduce the computational burden introduced by a multistep implementation, the proposed method is transformed into an equivalent optimization problem that can be solved by a fast SDA. Moreover, in [23] and [24], some CVVSs can be excluded in advance by adding the restrictions. However, it cannot be ensured that the final selected one by this search method is the optimal one with the minimum cost function value.

In this article, the predictive step of model predictive current control (MPCC) is increased so as to improve its control performance. And then, one simplified search method is proposed to exclude many unsuitable CVVSs in advance to reduce the complexity of multistep MPCC (M-MPCC). This simplified method is derived in the case of one predictive step, and then it is further extended to the case of two and *N* predictive horizons. Compared with the SDA method, the process of selecting a suitable radius is not needed and the no-solution case will not happen. In Section II, one simplified search method for the MPCC with one predictive step is described in detail. In Section III, when the predictive step is more than one, the reference voltage vector (RVV) in each predictive step, i.e., RVV sequence (RVVS), is derived so that many CVVSs can be excluded in advance under the guide of RVVS. Section IV makes full investigations on the characteristics of the proposed M-MPCC and discusses the influence of predictive steps on MPCC, which are verified by simulation and experiments. Finally, the conclusions is drawn in Section V.

II. Predictive Model of LIM

The model of LIM can be expressed in vector form, i.e., $X = x_\alpha + jx_\beta$, as following:

$$\begin{cases} \frac{dI_1}{dt} = \frac{L_r}{(L_rL_s - L_m^2)} \\ \quad (V_1 - (R_1 + \frac{R_2L_m^2}{L^2{}_r})I_1 + \frac{R_2L_m}{L^2{}_r}\psi_2 - j\frac{L_m}{L_r}\omega_2\psi_2) \\ \frac{d\psi_2}{dt} = \frac{R_2L_m}{L_r}I_1 - \frac{R_2}{L_r}\psi_2 + j\omega_2\psi_2 \end{cases} \quad (1)$$

where subscripts 1 and 2 represent the variables for the LIM primary and secondary, respectively. I_1 represents the primary current vector, ψ_2 represents the secondary flux vector, and V_1 represents the input primary voltage vector. L_m is the equivalent mutual inductance modified by the LEE factor *f*(*Q*) [4], ω_2 is the secondary angular velocity, *R* is the resistance, and L_s and L_r are the primary and secondary inductances, respectively.

In the digital controller, the predicted current vector can be achieved by the first-order Euler method, expressed as

$$\begin{aligned} I_1^{k+1} &= \left(1 - \frac{T_s(L^2{}_rR_1 + R_2L_m^2)}{(L^2{}_rL_s - L_rL_m^2)}\right) I_1^k \\ &\quad + \frac{L_rT_s}{(L_rL_s - L_m^2)}\left(V_1^k + \frac{R_2L_m}{L^2{}_r}\psi_2^k - j\frac{L_m}{L_r}\omega_2\psi_2^k\right) \\ &\Rightarrow I_1^{k+1} = MI_1^k + HV_1^k + L_\psi^k \end{aligned} \quad (2)$$

where the superscripts *k* and *k*+1 represent the variables at the *k*th and the (*k*+1)th time steps, respectively, T_s is the sampling period, $M = (1 - \frac{T_s(L^2{}_rR_1+R_2L_m^2)}{(L^2{}_rL_s-L_rL_m^2)})$, $H = \frac{L_rT_s}{(L_rL_s-L_m^2)}$, and $L_\psi^k = \frac{L_rT_s}{(L_rL_s-L_m^2)}(\frac{R_2L_m}{L^2{}_r}\psi_2^k - j\frac{L_m}{L_r}\omega_2\psi_2^k)$.

In order to compensate the delay caused by the online computing time, at the *k*th time step, it needs to further predict the current at the (*k*+1)th time step by (2), and then the optimal voltage vector (OVV) at the (*k*+1)th time step can be solved by the predicted current instead of the sampled current. The cost function can be expressed as

$$J = \left\|I_1^* - I_1^{k+2}\right\|^2 + k_{\rm sw}\left\|V_1^{k+1} - V_1^k\right\|^2 \quad (3)$$

where the first term evaluates the current tracking performance, the second term evaluates the switching effort, I_1^* is the reference current vector, and $k_{\rm sw}$ is the weighting factor to balance the current tracking and switching frequency penalty terms. By substituting (2) into (3), the cost function can be rewritten as

$$\begin{aligned} J &= (\frac{L_rT_s}{(L_rL_s - L_m^2)})^2 J_1 \\ \Rightarrow J_1 &= \left\|V_1^{k+1} - V_{k+1}^*\right\|^2 + \frac{k_{sw}(L_rL_s - L_m^2)^2}{(L_rT_s)^2}\left\|V_1^{k+1} - V_1^k\right\|^2 \\ \Rightarrow J_1 &= \left\|V_1^{k+1} - V_{k+1}^*\right\|^2 + \lambda\left\|V_1^{k+1} - V_1^k\right\|^2 \\ \Rightarrow J_1 &= (1+\lambda)\left\|V_1^{k+1} - \frac{V_{k+1}^* + \lambda V_1^k}{1+\lambda}\right\|^2 + Z_{k+1}^1 \end{aligned} \quad (4)$$

where V_{k+1}^* and Z_{k+1}^1 are defined in the Appendix.

Because the Z_{k+1}^1 is a constant value for different CVVs at the *k*th time step, in the case of one predictive step, the cost function can be simplified as

$$J_1' = \left\|V_1^{k+1} - \frac{V_{k+1}^* + \lambda V_1^k}{1+\lambda}\right\|^2 = \left\|V_1^{k+1} - U_{1(k+1)}^*\right\|^2. \quad (5)$$

According to (5), the cost function value is related to the distance between the CVV and the RVV $U_{1(k+1)}^*$. And thus, the output voltage plane of the two-level inverter is divided into seven sectors so as to simply compare the distance, as depicted in Fig. 1. As seen from this picture, it is obvious that the OVV is in the same sector of RVV, which can be directly selected by judging the sector of RVV with less calculation cost.

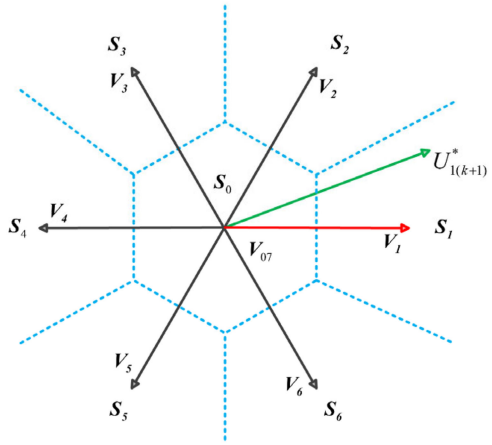

Fig. 1. Sectors of output voltage plane.

III. MPCC With Long Predictive Horizon

When the predictive step N_p is chosen as more than one, the optimal voltage vector sequence (OVVS) instead of a single OVV should be found. And the number of CVVs is increased from 7 to $N_p \times 7^{N_p}$. Therefore, it is necessary to remove some unsuitable CVVSs in advance so that the complexity of M-MPCC can be reduced. In this section, one small set that includes the optimal OVVS with the guide of RVVS is found to make the number of CVV in this set as small as possible. In order to illustrate it more clearly, the following derivation will start from two predictive steps.

A. N_p=2

In the case of two predictive steps, the cost function can be expressed as

$$J = \left\|I^*_{k+1} - I^{k+2}_1\right\|^2 + \left\|I^*_{k+2} - I^{k+3}_1\right\|^2 + k_{\rm sw}\left\|V^{k+1}_1 - V^k_1\right\|^2 + k_{\rm sw}\left\|V^{k+2}_1 - V^{k+1}_1\right\|^2. \quad (6)$$

Considering (4), (6) can be rewritten as

$$J = \left(\frac{L_r T_s}{(L_r L_s - L_m^2)}\right)^2 J_2$$
$$\Rightarrow J_2 = \left\|V^{k+1}_1 - V^*_{k+1}\right\|^2 + \left\|V^{k+2}_1 - V^*_{k+2}\right\|^2 + \lambda\{\left\|V^{k+1}_1 - V^k_1\right\|^2 + \left\|V^{k+2}_1 - V^{k+1}_1\right\|^2\}$$
$$\Rightarrow J_2 = \left\|V^{k+1}_1 - V^*_{k+1}\right\|^2 + \lambda\left\|V^{k+1}_1 - V^k_1\right\|^2 + (1+\lambda)\left\|V^{k+2}_1 - \frac{V^*_{k+2} + \lambda V^{k+1}_1}{1+\lambda}\right\|^2 + \frac{\lambda}{1+\lambda}\left\|V^*_{k+2} - V^{k+1}_1\right\|^2 \quad (7)$$

where

$$V^*_{k+2} = aI^{k+2}_1 + bI^*_{k+2} + D^{k+2}_\psi.$$

For simplicity, in the predictive horizon, it assumes that the secondary flux and angular velocity are almost unchanged, and the reference current vector in each step is the same as each other, i.e., $I^*_{k+2} = I^*_{k+1} = I^*_1$. And, considering (2), the vector V^*_{k+2} can be illustrated by

$$V^*_{k+2} = aI^{k+2}_1 + bI^*_1 + D^{k+1}_\psi$$
$$\Rightarrow V^*_{k+2} = a(MI^{k+1}_1 + HV^{k+1}_1 + L^{k+1}_\psi) + bI^*_1 + D^{k+1}_\psi$$
$$\Rightarrow V^*_{k+2} = AI^{k+1}_1 + BV^{k+1}_1 + G_{k+1}. \quad (8)$$

Substituting (8) into the last term in (7), it will get

$$J_2 = \left\|V^{k+1}_1 - V^*_{k+1}\right\|^2 + \lambda\left\|V^{k+1}_1 - V^k_1\right\|^2 + (1+\lambda)\left\|V^{k+2}_1 - \frac{V^*_{k+2} + \lambda V^{k+1}_1}{1+\lambda}\right\|^2 + \frac{\lambda(1-B)^2}{1+\lambda}\left\|V^{k+1}_1 - \frac{AI^{k+1}_1 + G_{k+1}}{1-B}\right\|^2. \quad (9)$$

And then, according to the following principle:

$$m_1\|X - X_1\|^2 + m_2\|X - X_2\|^2 + m_3\|X - X_3\|^2 = (m_1+m_2+m_3)\left\|X - \frac{m_1X_1 + m_2X_2 + m_3X_3}{m_1+m_2+m_3}\right\|^2 + \frac{m_3(m_1+m_2)}{m_1+m_2+m_3}\left\|\frac{m_1X_1 + m_2X_2}{m_1+m_2} - X_3\right\|^2 + \frac{m_1m_2}{m_1+m_2}\|X_1 - X_2\|^2 \quad (10)$$

the cost function (9) can be represented by

$$J_2 = \left(1 + \lambda + \frac{\lambda(1-B)^2}{1+\lambda}\right)\left\|V^{k+1}_1 - U^*_{2(k+1)}\right\|^2 + (1+\lambda)\left\|V^{k+2}_1 - U^*_{1(k+2)}\right\|^2 + Z^2_{k+1} \quad (11)$$

where

$$U^*_{2(k+1)} = \frac{V^*_{k+1} + \lambda V^k_1 + \frac{\lambda(1-B)^2}{1+\lambda}\frac{AI^{k+1}_1 + G_{k+1}}{1-B}}{1 + \lambda + \frac{\lambda(1-B)^2}{1+\lambda}}$$

$$U^*_{1(k+2)} = \frac{V^*_{k+2} + \lambda V^{k+1}_1}{1+\lambda}$$

$$\text{and } Z^2_{k+1} = \frac{\frac{\lambda(1-B)^2}{1+\lambda}(1+\lambda)}{1 + \lambda + \frac{\lambda(1-B)^2}{1+\lambda}}\left\|\frac{V^*_{k+1} + \lambda V^k_1}{1+\lambda} - V^1_{k+1}\right\|^2 + \frac{\lambda}{1+\lambda}\left\|V^*_{k+1} - V^k_1\right\|^2.$$

Therefore, the RVVs at the (k+1)th and the (k+2)th time are $U^*_{2(k+1)}$ and $U^*_{1(k+2)}$, respectively. When λ=0, the RVVs at the (k+1)th and the (k + 2)th time are V^*_{k+1} and V^*_{k+2}, respectively. Because the value of Z^2_{k+1} is the same as each other for different CVVSs, this term can be ignored when evaluating the cost function. And thus, according to (11), the OVVS can be selected from CVVSs, which is the closest to the RVVS $(U^*_{2(k+1)}, U^*_{1(k+2)})$. However, the value of $U^*_{1(k+2)}$ depends on the selection of the

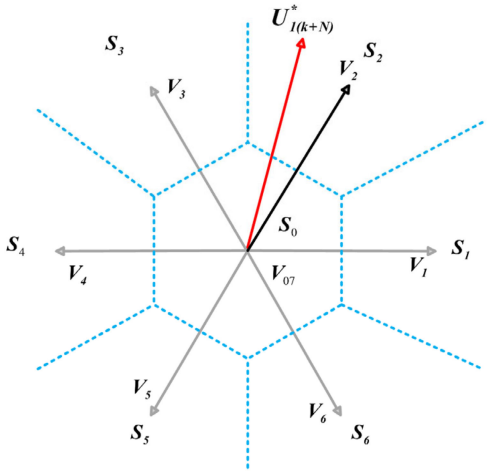

Fig. 2. Sectors at the last predictive step.

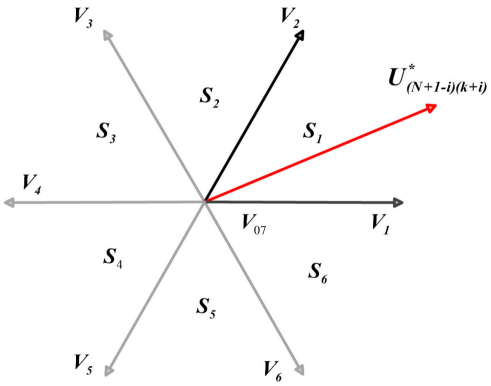

Fig. 3. Sectors at the early predictive steps.

first CVV V_1^{k+1}, and thus, it needs to enumerate seven different V_1^{k+1}, and then the second CVV V_1^{k+2} can be directly selected under the guide of $U^*_{1(k+2)}$, as shown in Fig. 2. In this case, the number of CVVs can be reduced from 2×7^2 to 2×7.

Furthermore, the weighting factor of the first term in (11) is larger than its second term, so the cost function value is more dependent on its first term, and some first CVVs V_1^{k+1} that are away from the $U^*_{2(k+1)}$ can be removed in advance. Only one zero voltage vector (ZVV) and two nonzero voltage vectors (NVVs) in the same sector of $U^*_{1(k+2)}$ are evaluated at the first predictive step, as shown in Fig. 3. Therefore, the CVVs can be further reduced from 14 to 6.

B. $N_p > 2$

Taking the same assumption for (8), the cost function of M-MPCC can be designed as

$$J = \sum_{i=1}^{N} \left\| I_1^* - I_1^{k+1+i} \right\|^2 + k_{\text{sw}} \sum_{i=1}^{N} \left\| V_1^{k+i} - V_1^{k+i-1} \right\|^2. \tag{12}$$

Similar to the case of one predictive step, the cost function can be rewritten by substituting (2) into (12), as expressed by

$$J = \left(\frac{L_r T_s}{(L_r L_s - L_m^2)} \right)^2 J_N$$

$$\Rightarrow J_N = \sum_{i=1}^{N} \left\| V_1^{k+i} - V_{k+i}^* \right\|^2 + \lambda \sum_{i=1}^{N} \left\| V_1^{k+i} - V_1^{k+i-1} \right\|^2. \tag{13}$$

In (13), the vector V^*_{k+i} can be illustrated by

$$V^*_{k+i} = aI_1^{k+i} + bI_1^* + D_\psi^{k+1}$$

$$\Rightarrow V^*_{k+i} = a(MI_1^{k+i-1} + HV_1^{k+i-1} + L_\psi^{k+1}) + bI_1^* + D_\psi^{k+1}$$

$$\Rightarrow V^*_{k+i} = AI_1^{k+i-1} + BV_1^{k+i-1} + G_{k+1}. \tag{14}$$

In order to deduce the RVVS, the recursive equation can be deduced as

$$l_1\|V - V_1\|^2 + \cdots + l_n\|V - V_n\|^2 = (l_1 + \cdots + l_n)$$

$$\left\| V - \frac{l_1V_1 + \cdots + l_nV_n}{l_1 + \cdots + l_n} \right\|^2$$

$$+ \frac{l_n(l_1 + \cdots + l_{n-1})}{l_1 + \cdots + l_n} \left\| \frac{l_1V_1 + \cdots + l_{n-1}V_{n-1}}{l_1 + \cdots + l_{n-1}} - V_n \right\|^2$$

$$+ \cdots + \frac{l_1l_2}{l_1 + l_2}\|V_1 - V_2\|^2. \tag{15}$$

The cost function can be further simplified by repeatedly using (2), (14), and (15), as described by

$$J_N = \sum_{i=1}^{N} K_i \left\| V_1^{k+i} - U^*_{(N+1-i)(k+i)} \right\|^2 + Z_{k+1}^N \tag{16}$$

where K_i , $U^*_{(N+1-i)(k+i)}$, and Z_{k+1}^N are defined in the Appendix.

The variable Z_{k+1}^N is also one unchanged value for different CVVSs, and thus, the cost function value depends on the distance between the CVVSs $(V_1^{k+1}, \ldots, V_1^{k+N})$ and the RVVS $(U^*_{N(k+1)}, \ldots, U^*_{1(k+N)})$, as described by

$$J'_N = \sum_{i=1}^{N} K_i \left\| V_1^{k+i} - U^*_{(N+1-i)(k+i)} \right\|^2. \tag{17}$$

According to (11), when the partial CVVSs $(V_1^{k+1}, \ldots, V_1^{k+N-1})$ are determined, the last one CVV in the CVVS V_1^{k+N} can be directly selected by judging the sector of $U^*_{1(k+N)}$, as described in Fig. 2. So, the maximum number of CVVs is reduced from $N \times 7^N$ to $N \times 7^{N-1}$.

Furthermore, the weighting factors in each step are different from each other and decrease with the predictive step, i.e., $K_1 > \cdots > K_N$, which is more important to minimize the value of terms at the early predictive steps. So, in order to ensure the value of cost function as small as possible, it only evaluates three adjacent CVVs at the early predictive steps, which are one ZVV and two NVVs in the same sector of RVVS, as depicted in Fig. 3. Finally, when the predictive step is selected as 4, Fig. 4 shows the

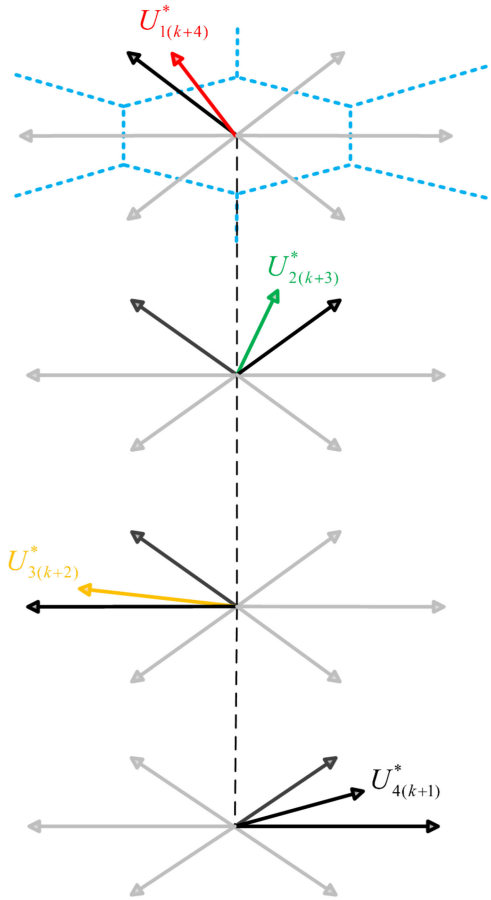

Fig. 4. Process of removing the CVVs by the simplified method.

execution process of excluding CCVs for this simplified search method, and the number of CVV can be further reduced to $N \times 3^{N-1}$.

C. Execution Process of the Proposed Method

In each predictive step, it needs to judge the sector of RVV, and then select the CVVs in the same sector. In order to avoid considering all possible cases in other sectors, the RVV can be transformed into Sector 1 by

$$T = \begin{bmatrix} \cos(\frac{(n-1)\pi}{3}) & \sin(\frac{(n-1)\pi}{3}) \\ -\sin(\frac{(n-1)\pi}{3}) & \cos(\frac{(n-1)\pi}{3}) \end{bmatrix} \tag{18}$$

where n represents the sector of RVV.

And then, in Fig. 5, the selected three CVVs can be further ranked based on the transformed RVV $\bar{U}^*_{(N+1-i)(k+i)}$, as described by

$$O_i = \begin{cases} \{V_n, V_{n+1}, V_0\} & X > 0, Y > 0 \\ \{V_n, V_{n-1}, V_0\} & X > 0, Y < 0 \\ \{V_0, V_n, V_{n+1}\} & X < 0, Y > 0 \\ \{V_0, V_n, V_{n-1}\} & X < 0, Y < 0 \end{cases} \tag{19}$$

where $X = \mathrm{Re}(\bar{U}^*_{(N+1-i)(k+i)}) - V_{\mathrm{dc}}/3$, $Y = \mathrm{Im}(\bar{U}^*_{(N+1-i)(k+i)})$, and V_{dc} is the dc-link voltage of the inverter. If $n = 1$, V_{n-1} is V_6; and if $n = 6$, V_{n+1} is V_1.

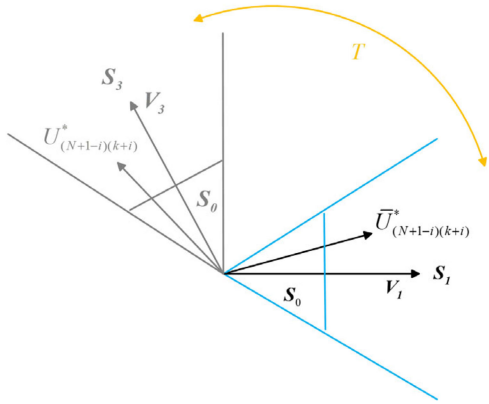

Fig. 5. Regions of the RVV.

Therefore, at the last predictive step, it only selects the first one CVV in (19), i.e., $O_N(1)$. Nevertheless, at the other predictive steps, it needs to evaluate three CVVs one by one based on the order of (19), i.e., $O_i(1, 2, 3)$. In this case, the CVV with the smaller cost function value at each predictive step has a higher priority in the search process. Thus, it is more possible to find the OVVS first. And then, the BAB method is combined with this simplified method so as to further reduce its online calculation time. The bound of this method may become very tight because the CVVS with the smaller cost function values is preferentially considered. Finally, the detailed execution flowchart of the proposed method is shown in Fig. 6(a). And, the dual closed-loop structure of the proposed method is illustrated in Fig. 6(b).

IV. Simulation and Experimental Results

This section presents the results of MPCC with one, three, and five predictive steps so as to analyze the relation between the performance of MPCC and the predictive step. In order to save the testing space, two coupled identical 3 kW arc induction motors (AIMs) are used to simulate the linear movement of an actual LIM [25], [26], as shown in Fig. 7. In order to simulate the linear motion more realistically and the severe end effect of the LIM used in the high-power traction applications, the diameter of the AIMs is designed as 1.23 m and the length of the secondary conductor plate is close to three times of the motor's primary length. The main parameters of AIMs used in both simulation and experiments are listed in Table I. The sampling frequency is chosen as 5 kHz, and the dc-link voltage is 300 V. The control unit used in the converter is DSP TMS320F28335.

A. Simulation and Analysis

The current vector reference I_1^* is set as $(0, 0)$, and the switching state at the previous time step is V_6. Under these testing conditions, in order to explain how the selected CVV will be influenced by predictive steps N_p and weighting factor λ, the solutions of MPCC with one and five predictive steps are described in Figs. 8 and 9, respectively. In these figures, the regions of OVV are distributed according to the sampled current vector I_1^k. When it neglects the switching frequency penalty term, i.e., $\lambda = 0$, the distributions of OVV with different

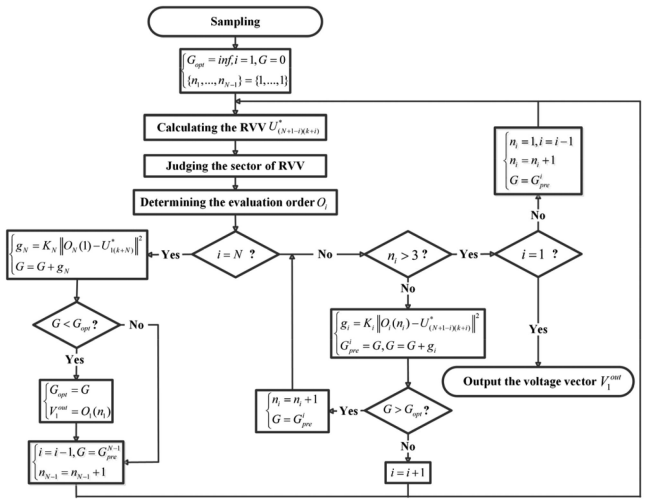

(a)

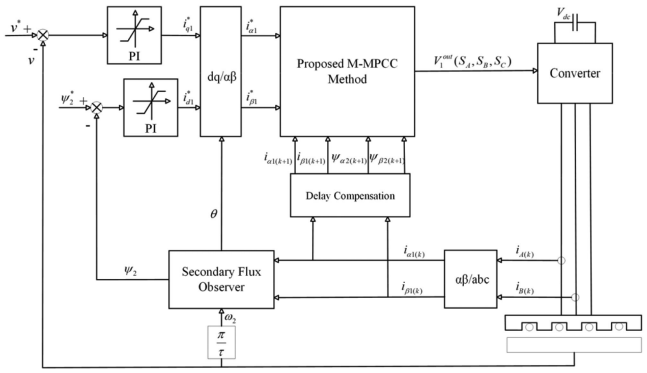

(b)

Fig. 6. Block diagram of the simplified method. (a) Execution flowchart. (b) Structure of control system.

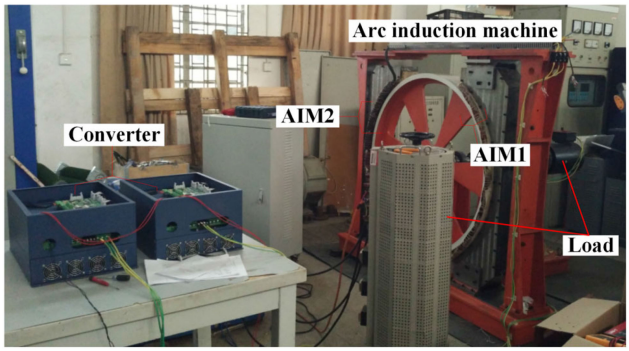

Fig. 7. LIM test platform comprised of two AIMs.

predictive steps are similar to each other, as shown in Figs. 8(a) and 9(a), respectively. Because there are no restrictions on the number of switching from the present to the future switching state, the selections of OVV are dependent on the current tracking errors so that the relation between the present and future switching state becomes less relevant. And thus, the predictive steps have less influence on the solutions of MPCC when the weighting factor λ is zero.

TABLE I
MAIN PARAMETERS OF TWO AIMS

Name	Symbol	Value and Unit
Primary pole pitch length	τ	0.1485 m
Primary length	l	1.3087 m
Primary leakage inductance	L_{l1}	11.09 mH
Secondary leakage inductance	L_{l2}	3.82 mH
Mutual inductance	L_m	31.73 mH
Primary resistance	R_1	1.47 Ω
Secondary resistance	R_2	1.61 Ω

However, because the selections of OVV partly depend on the previous switching state, the predictive steps will obviously change the distributions of OVV when $\lambda \neq 0$, as compared in Figs. 8(b) and 9(b), respectively. Moreover, in Fig. 8(c), when it further increases the value of λ, the OVV of MPCC with one predictive step is the switching state V_6 at the previous time step. In this case, the value of the current tracking term is negligible compared with the switching frequency penalty term, and thus, no voltage vector switch is the best choice. While, for the MPCC with five predictive steps, the OVV is not the fixed one in different regions, as described in Fig. 9(c). The more predictive steps can optimize the voltage vector sequence within the predictive horizon so as to reduce the number of switching in the future switching states. Therefore, the balance between the current tracking performance and the number of switching can be further enhanced by increasing the predictive step, and the weighting factor is not the only one factor that can influence the performance of M-MPCC.

Furthermore, when the predictive step is selected as three and five, the starting and braking processes of M-MPCC are tested in Fig. 10, where n represents the number of CVVs needed to be evaluate in one control circle. As can be seen, the current can be well controlled in both three and five predictive steps. Both the dynamic response and steady-state performance are satisfactory. In this figure, the simplified search method can find out the OVVS without mistakes, which is the same as that of the exhaustive enumeration method, i.e., $\Delta V = 0$. Compared with the traditional solution method, in the case of three predictive steps, the maximum number of CVV by this proposed method is reduced from 1029 to around 15, as shown in Fig. 10(a). Moreover, when the predictive step is selected as 5, except for the initial start-up process, the maximum number of CVV is reduced from 84035 to around 80, as shown in Fig. 10(b). Therefore, this proposed search method can effectively reduce the complexity of M-MPCC.

The complexity of multistep FCS-MPC is analyzed in detail, as shown in Fig. 11. When the predictive step is selected as 3, it needs to evaluate all possible 1029 CVVs by the traditional exhaustive search method, while this proposed search method can first find a small set that includes 27 CVVs with the help of

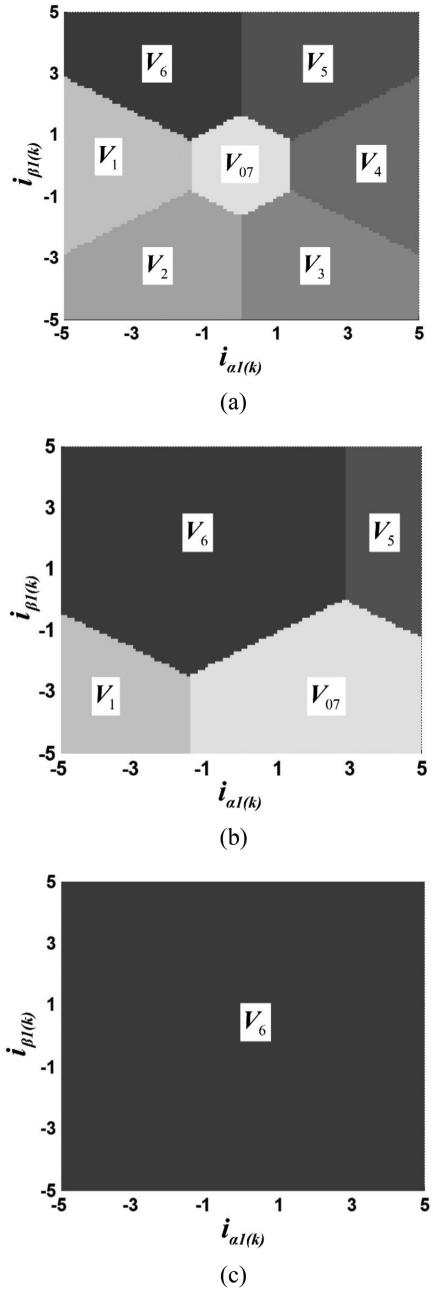

Fig. 8. Solutions of MPCC with one predictive step. (a) λ=0. (b) λ=3. (c) λ=6.

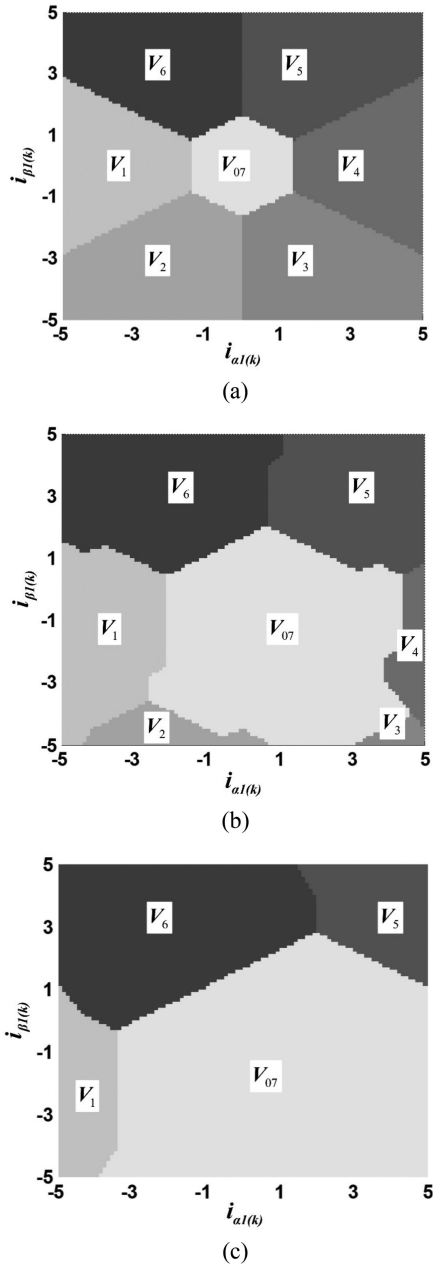

Fig. 9. Solutions of MPCC with five predictive steps. (a) λ=0. (b) λ=3. (c) λ=6.

RVVS, and then the BAB method with ranking operation can further reduce the number of CVV to 18 in the worst case and to 7 in the best case. The average number of CVV in evaluation is only 9, as described in Fig. 11(a). It can be seen that in the case of five predictive steps, the proposed search method is more effective. Fig. 11(b) shows that the maximum number of CVV by this method is 106, which occurs in the initial start-up process, while the traditional search method needs to evaluate 84 035 CVVs. Therefore, this simplified method can reduce the huge number of CVVs to a lower number so that the MPCC with more than one predictive step can be applied in practical applications. To evaluate the effectiveness of the ranking operation in Section III-B, the simulation results without ranking are added, as shown in Fig. 12. Compared with the simulation results with ranking in Fig. 11, it can be concluded that the ranking operation can improve the effect of the BAB method obviously.

B. Experimental Results and Analysis

The experimental results, including speed, phase current, and thrust, are given out in Fig. 13 in which the starting up and the braking process are implemented under a dual closed-loop control mode. The predictive step is set as 5 and the weighting factors as 0.5. The speed command value is given as 5 m/s

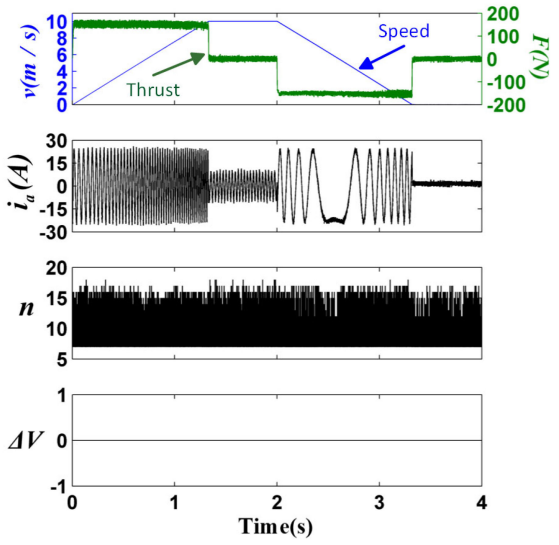

(a)

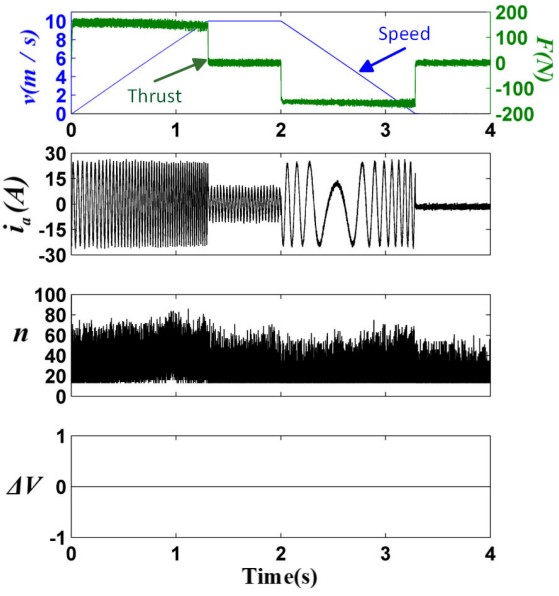

(b)

Fig. 10. Dynamic performance of the MPCC. (a) N_p=3. (b) N_p=5.

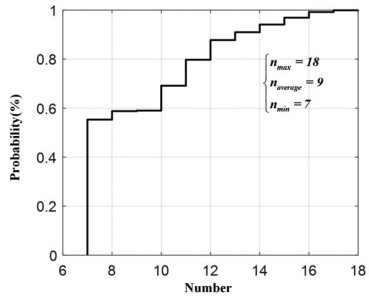

(a)

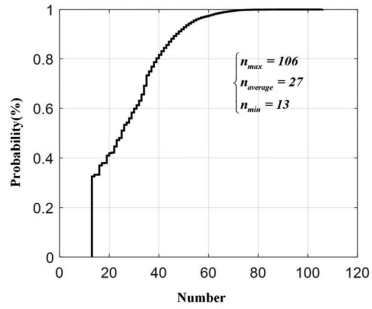

(b)

Fig. 11. Complexity of M-MPCC with ranking. (a) N_p=3. (b) N_p=5.

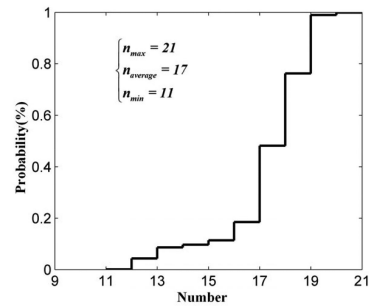

(a)

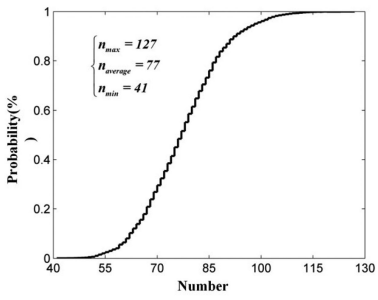

(b)

Fig. 12. Complexity of M-MPCC without ranking. (a) N_p=3. (b) N_p=5.

first and then decreases to 0 m/s after the motor speed enters the steady state. As can be seen, the motor speed can track the target value with good dynamic and static response. The current waveform is quite smooth and the motor thrust has a fast response.

In order to analyze the effect of switching frequency on the current THD, the switching frequency can be changed by adjusting the weighting factor λ. When the amplitude and frequency of current reference are set as 15 A and 30 Hz, respectively, the relation between the switching frequency and the current THD is compared in Fig. 14. As seen from this figure, the current THD will increase with the decreasing switching frequency, and more predictive steps will bring better quality of current. Furthermore, the current THDs of MPCC with different predictive steps are compared under the same switching frequency, as depicted in Fig. 15. When the switching frequency is selected as 1100 Hz, i.e., $\lambda = 0$ for the MPCC with different predictive steps, the current THDs of different MPCC methods are almost the same as each other. However, the difference becomes more significant in the case of the lower switching frequency, i.e., $\lambda \neq 0$. Therefore, it is more meaningful to increase the predictive steps of MPC

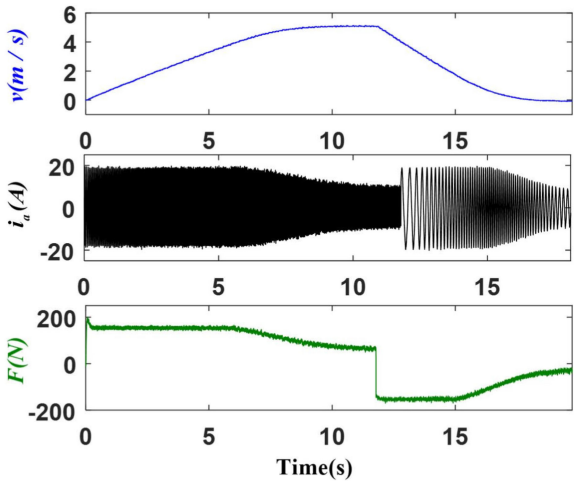

Fig. 13. Dynamic response of the proposed M-MPCC.

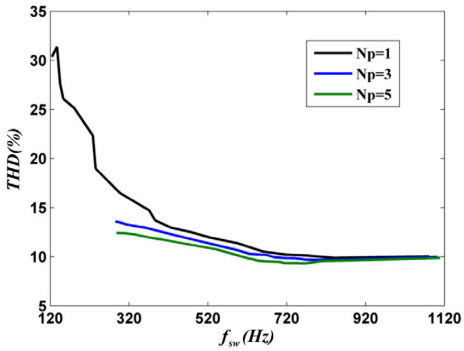

Fig. 14. Comparative current THDs under the different switching frequencies.

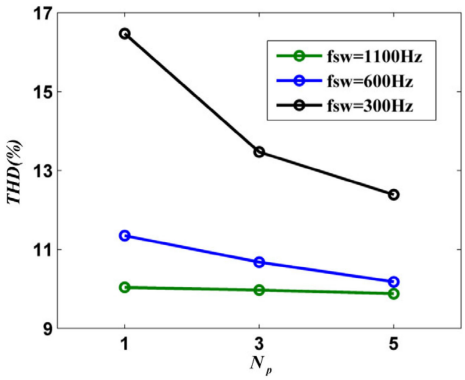

Fig. 15. Comparative current THDs under the same switching frequencies.

when the switching frequency is controlled as the low value by the large weighting factor.

The square current tracking errors quantifying the tracking performance of M-MPCC are defined as

$$M = \sum_{i=1}^{l} \frac{\|I_1^* - I_1\|_i^2}{l} \tag{20}$$

where l is the total number of sampling points.

Moreover, in the case of different weighting factors, the switching frequencies and the current tracking errors of MPCC

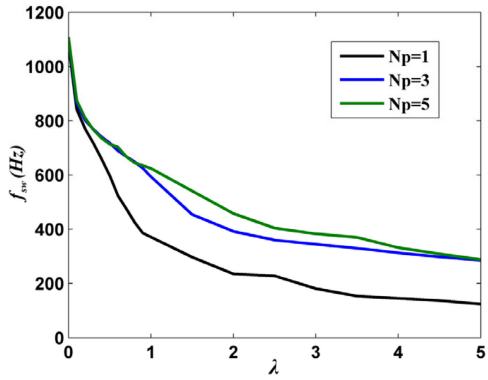

Fig. 16. Comparative switching frequencies with different weighting factors.

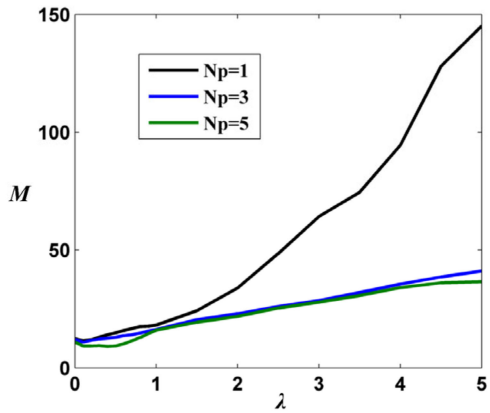

Fig. 17. Comparative current tracking errors with different weighting factors.

TABLE II
CALCULATION TIME OF THE MPCC WITH DIFFERENT PREDICTIVE STEPS

Predictive step	Calculation time
1	75.6μs
3	140.8μs
5	194.7μs

with one, three, and five predictive steps are compared as shown in Figs. 16 and 17, respectively. As seen from these figures, both the switching frequencies and tracking errors of MPCC with one predictive step are more sensitive to the variations of weighting factor compared with the other two methods. When the weighting factors are same, the MPCC with more predictive steps can achieve the smaller tracking errors, while the higher switching frequencies. However, the differences of these MPCC methods are not obvious in the case of a small weighting factor.

Finally, the online calculation time of MPCC with one, three, and five predictive steps is tested in this article, as listed in Table II. The MPCC with one predictive step can directly find the OVV by judging the sector of RVV, and thus, its calculation time is the shortest compared with the MPC with three and five

predictive steps. Although the calculation time of MPCC will obviously increase with its predictive steps, its complexity can be effectively reduced by the simplified search method, which can finish the program of M-MPCC within 200 μs in practice. Therefore, with the help of this proposed search method, the M-MPCC can be implemented in the microprocessor with a low calculation cost.

V. Conclusion

In order to reduce the complexity of M-MPCC, one simplified search method is proposed in this article. First, this method can find the small CVVS set with the help of RVVS, which can exclude the large number of CVVS in advance. And then, the remaining CVVS can be ranked by judging the region of RVVS, so it gives the higher priority to evaluate the CVVS with the smaller cost function values in the search process. By combining with the BAB method, it can reduce the number of CVV in the small set to a very low number because the ranked CVVS can make the bound very tight. Finally, both simulation and experimental results verify the effectiveness of this simplified method in which the current THDs of MPCC can be further reduced by increasing its predictive steps, especially at the low switching frequency. Therefore, the M-MPCC can further optimize the relation between the switching frequency and current THD, which can find the potential applications in the high-power drive systems.

Appendix

The variables used in (4) are expressed as

$$\begin{aligned} V^*_{k+1} &= \left(\frac{L^2{}_r R_1 + R_2 L_m^2}{L^2{}_r} - \frac{L_r L_s - L_m^2}{L_r T_s}\right) I_1^{k+1} \\ &+ \frac{L_r L_s - L_m^2}{L_r T_s} I_1^* \\ &- \frac{R_2 L_m}{L^2{}_r}\psi_2^{k+1} + j\frac{L_m}{L_r}\omega_2 \psi_2^{k+1} \\ &\Rightarrow V^*_{k+1} = aI_1^{k+1} + bI_1^* + D_\psi^{k+1} \end{aligned} \tag{A-1}$$

$$Z^1_{k+1} = \frac{\lambda}{1+\lambda}\left\|V^*_{k+1} - V_1^{\mathrm{k}}\right\|^2. \tag{A-2}$$

The variables in (10) are defined by

$$\begin{cases} K_1 = 1 + \lambda + k_1 + \cdots + k_{N-1} \\ \cdots \\ K_{N-1} = 1 + \lambda + k_1 \\ K_N = 1 + \lambda \end{cases} \tag{A-3}$$

$$\text{where } k_i = \begin{cases} k_1 = \frac{\lambda(1-B)^2}{1+\lambda} \\ k_2 = \frac{k_1(1+\lambda)}{1+\lambda+k_1} K_{2V}^2 \\ k_i = \frac{k_{i-1}(1+\lambda+k_1+\cdots+k_{i-2})}{1+\lambda+k_1+\cdots+k_{i-1}} K_{iV}^2 \ (i \geq 3). \end{cases}$$

$$U^*_{(N+1-i)(k+i)} = \begin{cases} \frac{V^*_{k+N} + \lambda V_1^{k+N-1}}{1+\lambda} & (i = N) \\ \frac{V^*_{k+i} + \lambda V_1^{k+i-1} + k_1 V_{k+i}^1 + \cdots + k_{N-i} V_{k+i}^{N-i}}{1+\lambda+k_1+\cdots+k_{N-i}} & (i < N) \end{cases} \tag{A-4}$$

$$\text{where } V_{k+i}^{N-i} = \frac{K_{(N-i)I} I_1^{k+i} + K_{(N-i)G} G_{k+1} + K_{(N-i)L} L_\psi^{k+1}}{K_{(N-i)V}}.$$

The defined variables $K_{hV}, K_{h\mathrm{I}}, K_{hG},$ and K_{hL} can be calculated by the following iteration law, as expressed by

$$\begin{cases} K_{1V} = 1 - B \\ K_{2V} = \frac{K_{1I} H}{K_{1V}} - \frac{B+\lambda}{1+\lambda} \\ \cdots \\ K_{hV} = \frac{K_{(h-1)I} H}{K_{(h-1)V}} - \frac{B+\lambda}{1+\lambda+k_1+\cdots+k_{h-2}} \\ \qquad - \sum_{i=1}^{h-2} \frac{K_{iI} H}{K_{iV}} \frac{k_i}{1+\lambda+k_1+\cdots+k_{h-2}} \end{cases} \tag{A-6}$$

$$\begin{cases} K_{1I} = A \\ K_{2I} = \frac{A}{1+\lambda} - \frac{K_{1I} M}{K_{1V}} \\ \cdots \\ K_{hI} = \frac{A}{1+\lambda+k_1+\cdots+k_{h-2}} - \frac{K_{(h-1)I} M}{K_{(h-1)V}} \\ \qquad + \sum_{i=1}^{h-2} \frac{K_{iI} M}{K_{iV}} \frac{k_i}{1+\lambda+k_1+\cdots+k_{h-2}} \end{cases} \tag{A-7}$$

$$\begin{cases} K_{1G} = 1 \\ K_{2G} = \frac{1}{1+\lambda} - \frac{K_{1G}}{K_{1V}} \\ \cdots \\ K_{hG} = \frac{1}{1+\lambda+k_1+\cdots+k_{h-2}} - \frac{K_{(h-1)G}}{K_{(h-1)V}} \\ \qquad + \sum_{i=1}^{h-2} \frac{K_{iG}}{K_{iV}} \frac{k_i}{k_1+\cdots+k_{n-2}} \end{cases} \tag{A-8}$$

$$\begin{cases} K_{1L} = 0 \\ K_{2L} = -\frac{K_{1I} + K_{1L}}{K_{1V}} \\ \cdots \\ K_{hL} = \sum_{i=1}^{h-2} \frac{K_{iI} + K_{iL}}{K_{iV}} \frac{k_i}{1+\lambda+k_1+\cdots+k_{h-2}} - \frac{K_{(h-1)I} + K_{(h-1)L}}{K_{(h-1)V}}. \end{cases} \tag{A-9}$$

References

[1] J. Zou, W. Xu, X. Yu, Y. Liu, and C. Ye, "Multistep model predictive control with current and voltage constraints for linear induction machine based urban transportation," *IEEE Trans. Veh. Technol.*, vol. 66, no. 12, pp. 10817–10829, Dec. 2017.

[2] I. Boldea, L. N. Tutelea, W. Xu, and M. Pucci, "Linear electric machines, drives and MAGLEVs: An overview," *IEEE Trans. Ind. Electron.*, vol. 65, no. 9, pp. 7504–7515, Sep. 2018.

$$Z^N_{k+1} = \begin{cases} \frac{\lambda}{1+\lambda}\left\|V^*_{k+1} - V_1^{\mathrm{k}}\right\|^2 & (N=1) \\ \frac{\lambda}{1+\lambda}\left\|V^*_{k+1} - V_1^k\right\|^2 + \frac{k_1(1+\lambda)}{1+\lambda+k_1}\left\|\frac{V^*_{k+1} + \lambda V_1^k}{1+\lambda} - V_{k+1}^1\right\|^2 & (N=2) \\ Z^2_{k+1} + \sum_{i=2}^{N-1} \frac{k_i(1+\lambda+k_1+\cdots+k_{i-1})}{1+\lambda+k_1+\cdots+k_i}\left\|U^*_{i(k+1)} - V_{k+1}^i\right\|^2 & (N \geq 3) \end{cases}. \tag{A-5}$$

[3] G. Lv, T. Zhou, D. Zeng, and Z. Liu, "Influence of secondary constructions on transverse forces of linear induction motors in curve rails for urban rail transit," *IEEE Trans. Ind. Electron.*, vol. 66, no. 6, pp. 4231–4239, Jun. 2019.
[4] W. Xu, M. R. Islam, and M. Pucci, *Advanced Linear Machines and Drive Systems*. Berlin, Germany: Springer, 2019.
[5] J. Duncan, "Linear induction motor—Equivalent-circuit model," *IEE Proc. B - Electr. Power Appl.*, vol. 130, no. 1, pp. 51–57, Jan. 1983.
[6] M. Pucci, "State space-vector model of linear induction motors," *IEEE Trans. Ind. Appl.*, vol. 50, no. 1, pp. 195–207, Jan./Feb. 2014.
[7] W. Xu *et al.*, "Equivalent circuits for single-sided linear induction motors," *IEEE Trans. Ind. Appl.*, vol. 46, no. 6, pp. 2410–2423, Nov./Dec. 2010.
[8] W. Xu, G. Sun, G. Wen, Z. Wu, and P. K. Chu, "Equivalent circuit derivation and performance analysis of a single-sided linear induction motor based on the winding function theory," *IEEE Trans. Veh. Technol.*, vol. 61, no. 4, pp. 1515–1525, May 2012.
[9] G. Lv, D. Zeng, and T. Zhou, "An advanced equivalent circuit model for linear induction motors," *IEEE Trans. Ind. Electron.*, vol. 65, no. 9, pp. 7495–7503, Sep. 2018.
[10] G. Kang and K. Nam, "Field-oriented control scheme for linear induction motor with the end effect," *IEE Proc. - Electr. Power Appl.*, vol. 152, no. 6, pp. 1565–1572, Nov. 2005.
[11] K. Wang, Y. Li, Q. Ge, and L. Shi, "An improved indirect field-oriented control scheme for linear induction motor traction drives," *IEEE Trans. Ind. Electron.*, vol. 65, no. 12, pp. 9928–9937, Dec. 2018.
[12] H. Karimi, S. Vaez-Zadeh, and F. R. Salmasi, "Combined vector and direct thrust control of linear induction motors with end effect compensation," *IEEE Trans. Energy Convers.*, vol. 31, no. 1, pp. 196–205, Mar. 2016.
[13] J. Zou, W. Xu, J. Zhu, and Y. Liu, "Low-complexity finite control set model predictive control with current limit for linear induction machines," *IEEE Trans. Ind. Electron.*, vol. 65, no. 12, pp. 9243–9254, Dec. 2018.
[14] W. Xu, J. Zou, Y. Liu, and J. Zhu, "Weighting factorless model predictive thrust control for linear induction machine," *IEEE Trans. Power Electron.*, vol. 34, no. 10, pp. 9916–9928, Oct. 2019.
[15] C. Xia, T. Liu, T. Shi, and Z. Song, "A simplified finite-control-set model-predictive control for power converters," *IEEE Trans. Ind. Inform.*, vol. 10, no. 2, pp. 991–1002, May 2014.
[16] Y. Zhang and W. Xie, "Low complexity model predictive control—Single vector-based approach," *IEEE Trans. Power Electron.*, vol. 29, no. 10, pp. 5532–5541, Oct. 2014.
[17] M. J. Duran, J. Prieto, F. Barrero, and S. Toral, "Predictive current control of dual three-phase drives using restrained search techniques," *IEEE Trans. Ind. Electron.*, vol. 58, no. 8, pp. 3253–3263, Aug. 2011.
[18] T. Geyer and D. E. Quevedo, "Multistep finite control set model predictive control for power electronics," *IEEE Trans. Power Electron.*, vol. 29, no. 12, pp. 6836–6846, Dec. 2014.
[19] T. Geyer, "Computationally efficient model predictive direct torque control," *IEEE Trans. Power Electron.*, vol. 26, no. 10, pp. 2804–2816, Oct. 2011.
[20] P. Karamanakos, T. Geyer, and R. P. Aguilera, "Long-horizon direct model predictive control: Modified sphere decoding for transient operation," *IEEE Trans. Ind. Appl.*, vol. 54, no. 6, pp. 6060–6070, Nov./Dec. 2018.
[21] R. Baidya, R. P. Aguilera, P. Acuna, S. Vazquez, and H. du Toit Mouton, "Multistep model predictive control for cascaded H-bridge inverters: Formulation and analysis," *IEEE Trans. Power Electron.*, vol. 33, no. 1, pp. 876–886, Jan. 2018.
[22] P. Acuna, C. A. Rojas, R. Baidya, R. P. Aguilera, and J. E. Fletcher, "On the impact of transients on multistep model predictive control for medium-voltage drives," *IEEE Trans. Power Electron.*, vol. 34, no. 9, pp. 8342–8355, Sep. 2019.
[23] C. Xia, Z. Zhou, Z. Wang, Y. Yan, and T. Shi, "Computationally efficient multi-step direct predictive torque control for surface-mounted permanent magnet synchronous motor," *IET Electr. Power Appl.*, vol. 11, no. 5, pp. 805–814, May 2017.
[24] M. Votava, T. Glasberger, V. Smidl, and Z. Peroutka, "Improved model predictive control with extended horizon for dual inverter with real-time minimization of converter power losses," in *Proc. IEEE Int. Symp. Predictive Control Elect. Drives Power Electron.*, 2017, pp. 48–53.
[25] A. Majumdar and T. K. Bhattacharya, "Comparison of force developed in a linear induction machine and an equivalent arc linear induction machine at zero velocity," in *Proc. IEEE Int. Conf. Power Electron., Drives Energy Syst.*, 2018, pp. 1–5.
[26] W. Xu, J. G. Zhu, Y. Zhang, Y. Li, Y. Wang, and Y. Guo, "An improved equivalent circuit model of a single-sided linear induction motor," *IEEE Trans. Veh. Technol.*, vol. 59, no. 5, pp. 2277–2289, Jun. 2010.

Wei Xu (Senior Member, IEEE) received the double B.E. and M.E. degrees from Tianjin University, Tianjin, China, in 2002 and 2005, respectively, and the Ph.D. degree from the Institute of Electrical Engineering, Chinese Academy of Sciences, Beijing, China, in 2008, all in electrical engineering.

From 2008 to 2012, he was a Postdoctoral Fellow with the University of Technology Sydney, a Vice-Chancellor Research Fellow with the Royal Melbourne Institute of Technology, and a Japan Science Promotion Society Invitation Fellow with Meiji University. Since 2013, he has been a Full Professor with the State Key Laboratory of Advanced Electromagnetic Engineering, Huazhong University of Science and Technology, Wuhan, China. His research topics mainly cover the design and control of linear machines and drive systems. He has more than 110 papers accepted or published in IEEE transactions journals, two edited books published by Springer Press, one monograph published by China Machine Press, and more than 140 Invention Patents granted or pending, all in the related fields of electrical machines and drives.

Dr. Xu is a fellow of the Institute of Engineering and Technology. He will serve as the General Chair for the 2021 International Symposium on Linear Drives for Industry Applications and the 2023 IEEE International Conference on Predictive Control of Electrical Drives and Power Electronics in Wuhan, China. He has served as an Associate Editor for several IEEE transactions journals, such as the IEEE TRANSACTIONS ON INDUSTRIAL ELECTRONICS, and so on.

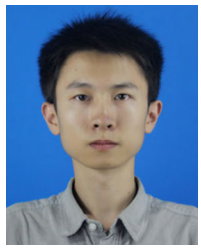

Dinghao Dong received the B.E. degree in electrical engineering from Wuhan University, Wuhan, China, in 2017. He is currently working toward the Ph.D. degree with the School of Electrical Engineering, Huazhong University of Science and Technology, Wuhan, China.

His current research interests include the control of brushless doubly fed induction generators, parameter identification, and model predictive control of linear induction motors.

Jianqiao Zou was born in Jiangxi, China, on July 30, 1993. He received the B.S. and Ph.D. degrees from the School of Electrical and Electronic Engineering, Huazhong University of Science and Technology, Wuhan, China, in 2015 and 2020, respectively.

His research interests include linear induction machine control, permanent magnet synchronous machine control, and model predictive control.

Yi Liu (Senior Member, IEEE) received the B.E. and M.E. degrees in automation and control engineering from the Wuhan University of Science and Technology, Wuhan, China, in 2004 and 2007, respectively, and the Ph.D. degree in mechatronic engineering from the Huazhong University of Science and Technology, Wuhan, China, in 2016.

From March 2016 to June 2016, he was a Senior R&D Engineer with the Fourth Academy of China Aerospace Science and Industry Corporation, Wuhan, China. From July 2016 to October 2019, he was a Postdoctoral Research Fellow with the State Key Laboratory of Advanced Electromagnetic Engineering and Technology, Huazhong University of Science and Technology, where he has been a Lecturer since January 2020. He is the Vice-Chair for IEEE IES Wuhan Chapter. He has authored or coauthored more than 30 high-quality SCI-indexed International journal papers, held more than 20 granted/pending invention patents, and one book on the control of brushless doubly fed inductor generators. His current research interests include multiport electrical machines and drive systems.

Dr. Liu has been invited to give tutorials on brushless DFIG for two conferences, i.e., the 2019 IEEE International Conference on Electrical Machines and Systems (ICEMS2019) and the 23rd China Power Supply Society Conference. And, he has organized special sessions on multiport electrical machines for four conferences, i.e., ICEMS2019, ECCE Asia2020, ICEM2020, and IEEE-PEMC2020.